Global Concentrations of CO₂ and CH₄ Retrieved from GOSAT: First Preliminary Results

T. Yokota, Y. Yoshida, N. Eguchi, Y. Ota, T. Tanaka, H. Watanabe, and S. Maksyutov
National Institute for Environmental Studies, Tsukuba, Japan

Abstract

The Greenhouse Gases Observing Satellite (GOSAT) was launched on January 23, 2009, to monitor global atmospheric levels of CO_2 and CH_4 from space. GOSAT started initial operation of its instruments after an initial satellite system check. Although the radiant data obtained by the GOSAT instruments are currently in the preliminary stages of calibration and validation, the spectral absorption features of CO_2 and CH_4 are clearly identifiable. An initial retrieval of these gaseous concentrations was performed for measurement scenes of cloud-free conditions over land. These results showed that column-averaged dry air mole fractions of both CO_2 and CH_4 in the northern hemisphere were higher than those in the southern hemisphere. These latitudinal differences agree with data obtained from ground-based sources and other satellite observations; however, the absolute values of the gaseous concentrations from GOSAT data seem to have been underestimated. Calibrations as well as validation should be conducted to improve the quality of GOSAT retrievals.

1. Introduction

The levels of total atmospheric carbon dioxide (CO_2) and methane (CH_4) have been increasing since the beginning of the industrial era. The level of CO_2 in particular has increased from the pre-industrial global level of 280 ppmv to 379 ppmv in 2005, most probably because of human activities (IPCC 2007). Satellite measurement is one of the most effective approaches to high spatio-temporal-resolution monitoring of global greenhouse gas distribution. The Japanese Ministry of the Environment (MOE), the National Institute for Environmental Studies (NIES) and the Japan Aerospace Exploration Agency (JAXA) jointly developed the Greenhouse Gases Observing Satellite (GOSAT; Yokota et al. 2004) to monitor global levels of CO_2 and CH_4 from space. GOSAT was launched on January 23, 2009, into a sun-synchronous orbit at an altitude of 666 km, coming back to the same location with a 3-days period. This paper shows the initial results of CO_2 and CH_4 column-averaged dry air mole fraction (X_{CO2} and X_{CH4}) from the GOSAT radiant spectrum data obtained under cloud-free conditions over land for April 20–28, 2009. Section 2 provides a brief description of the GOSAT instruments and retrieval method. Section 3 describes the results and Section 4 gives the current GOSAT status and concluding remarks.

2. Retrieval method

2.1 GOSAT instruments

GOSAT is equipped with two sensors; the Thermal and Near-infrared Sensor for Carbon Observation-Fourier Transform Spectrometer (TANSO-FTS) and the Cloud and Aerosol Imager (TANSO-CAI) (Kuze et al. 2006). TANSO-FTS detects short-wavelength infrared (SWIR) light reflected from the earth's surface, along with the thermal infrared (TIR) radiation emitted from the ground and atmosphere. It has three narrow bands in the SWIR region (0.76, 1.6, and 2.0 μm) and a wide TIR band (5.5–14.3 μm) at a spectral resolution of about 0.2 cm⁻¹ (Table 1). The TANSO-FTS instantaneous field of view (IFOV) is 15.8 mrad, corresponding to a nadir footprint diameter of 10.5 km. TANSO-CAI has four narrow bands in the near-ultraviolet to near-infrared region at 0.38, 0.674, 0.87, and 1.6 μm with a higher spatial resolution than TANSO-FTS (Table 2). TANSO-CAI can detect optically thick clouds inside the TANSO-FTS IFOV (Nakajima et al. 2008), and correct the effect of aerosols in the TANSO-FTS spectrum data.

2.2 Retrieval strategy of X_{CO2} and X_{CH4} from TANSO-FTS SWIR spectrum data

The radiance data obtained from both TANSO-FTS and TANSO-CAI are currently in the preliminary calibration stage, and the retrieval method used in this study is the same as will be used for operational GOSAT processing to provide official GOSAT data products to the public. In this paper, we retrieved X_{CO2} and X_{CH4} using only the TANSO-FTS 1.6 μm band. We selected the TANSO-FTS SWIR spectrum data with a signal-to-noise ratio (SNR) greater than 100 under cloud-free conditions as follows. The TANSO-FTS measurement scenes con-

Table 1. GOSAT TANSO-FTS Specifications.

Band	Band 1	Band 2	Band 3	Band 4
Polarization	P, S	P, S	P, S	–
Wavenumber range [cm⁻¹]	12900~ 13200	5800~ 6400	4800~ 5200	700~ 1800
FWHM of the ILSF	0.6 cm⁻¹ or less	0.27 cm⁻¹ or less	0.27 cm⁻¹ or less	0.27 cm⁻¹ or less
SNR	> 300[1]	> 300[1]	> 300[1]	> 300[2]
Target species	O_2	CO_2, CH_4	CO_2, H_2O	CO_2, CH_4
IFOV/FOV at nadir	IFOV: 15.8 mrad FOV for observation: diameter of app. 10.5 km			
data acquisition time	1.1, 2.0, 4.0 seconds (nominal: 4 sec.) for single-scan			

1) for Lambertian surface albedo of 0.3 at a solar zenith angle of 30 degree
2) at wavenumber of 700 cm⁻¹ for the incident blackbody radiation corresponding to 280 K

Table 2. GOSAT TANSO-CAI Specifications.

Band	Band 1	Band 2	Band 3	Band 4
Spectral coverage	0.370~ 0.390 μm	0.664~ 0.684 μm	0.860~ 0.880 μm	1.555~ 1.645 μm
SNR[1]	> 200	> 200	> 200	> 200
Swath	1000 km	1000 km	1000 km	750 km
Spatial resolution	0.5 km	0.5 km	0.5 km	1.5 km
Target substance	Cloud, Aerosol			

1) for Lambertian surface albedo of 0.3 at a solar zenith angle of 30 degree

taminated by elevated scattering particles (e.g., high clouds, including optically thin cirrus) were excluded using the absorption-saturated band of water vapor inside the TANSO-FTS 2.0 μm band. TANSO-FTS measurement scenes with optically thick clouds detected by TANSO-CAI were removed. The TANSO-CAI cloud detection algorithm consists of several threshold tests, the details of which have been reported by Nakajima et al. (2008). However, the TANSO-FTS measurement scenes could still be contaminated by clouds because the geometric calibration between TANSO-FTS and TANSO-CAI is still underway.

X_{CO2} and X_{CH4} were retrieved from the 1.6-μm CO_2 absorption band and the 1.67-μm CH_4 absorption band, respectively, using the optimal estimation method (Rodgers 2000). An optimal estimation of $\mathbf{x}$ was selected to minimize the cost and penalty function, defined as

$$J(\mathbf{x}) = [\mathbf{y} - \mathbf{F}(\mathbf{x})]^T \mathbf{S}_\varepsilon^{-1}[\mathbf{y} - \mathbf{F}(\mathbf{x})] + (\mathbf{x} - \mathbf{x}_a)^T \mathbf{S}_a^{-1}(\mathbf{x} - \mathbf{x}_a), \qquad (1)$$

where $\mathbf{x}$ is the state vector to be retrieved, $\mathbf{x}_a$ is the a priori state of $\mathbf{x}$, $\mathbf{S}_a$ is the a priori covariance matrix, $\mathbf{y}$ is the vector comprising the observed spectrum, $\mathbf{S}_\varepsilon$ is the error covariance matrix of the observed spectrum, and $\mathbf{F}(\mathbf{x})$ denotes the forward model that relates the state vector to the observed spectrum. The optimal estimation of $\mathbf{x}$ was obtained from the following iterative equation

$$\mathbf{x}_{i+1} = \mathbf{x}_i + (\mathbf{K}_i^T \mathbf{S}_\varepsilon^{-1}\mathbf{K}_i + \mathbf{S}_a^{-1} + \lambda_i \mathbf{D}^2)$$
$$\cdot \{\mathbf{K}_i^T \mathbf{S}_\varepsilon^{-1}[\mathbf{y} - \mathbf{F}(\mathbf{x}_i)] + \mathbf{S}_a^{-1}(\mathbf{x}_i - \mathbf{x}_a)\}, \qquad (2)$$

where the subscript i denotes the index of the ith iteration; $\mathbf{K}$ is the Jacobian matrix, which is the derivative of the forward model as a function of the state vector $\mathbf{x}$, i.e. $\mathbf{K} = \partial \mathbf{y}/\partial \mathbf{x}$; λ is chosen at each step to minimize the cost function; and $\mathbf{D}$ is a diagonal scaling matrix. The HITRAN 2008 database (Rothman et al. 2009) was used as the molecular spectroscopic parameter database. Spectrum data around the Fraunhofer lines of the solar spectrum were masked in the retrieval analysis to suppress the bias error. Additionally, spectrum data around water vapor lines were masked in the X_{CO2} retrieval, while the water vapor was retrieved along with X_{CH4}.

In the retrieval of X_{CO2} and X_{CH4}, the gaseous profiles of interest were retrieved first, and then the column abundances were obtained as the final outputs (Rodgers and Connor 2003). The column abundance of dry air was calculated from the surface pressure and water vapor profile of the operational analysis data named Grid Point Value (GPV) data provided by the Japan Meteorological Agency (JMA). Additionally, the ground

surface albedo, aerosol optical thickness, relative radiometric calibration adjustment factor, and water vapor profile (for X_{CH4} only) were included in the state vector as an auxiliary parameter and retrieved simultaneously. The a priori profiles of CO_2 and CH_4 were calculated for every observed day by an offline global atmospheric transport model, developed by NIES (hereafter called as NIES TM; Maksyutov et al. 2008) with GPV data as inputs. Climatological flux datasets based on the work of Law et al. (2008) and Patra et al. (2009) were used for CO_2 and CH_4 simulations, respectively. The model framework was evaluated against other models in the CO_2 intercomparison experiment, described by Law et al. (2008) and Patra et al. (2008). The a priori monthly variance and covariance matrices of CO_2 and CH_4 were derived from the simulated concentrations of NIES TM and analyzed datasets of GLOBALVIEW-CO2 (2008) and GLOBALVIEW-CH4 (2008) for each NIES TM grid point (see Eguchi et al. 2009 for the detail of making a priori covariance matrices). Covariance matrices for CO_2 and CH_4 profiles were multiplied by a factor of $(10)^2$ (tentative value) in the retrieval analysis. For the X_{CH4} retrieval, the a priori profile of water vapor was obtained from the near real-time forecasting GPV data and its covariance was evaluated from the water vapor profile of the GPV dataset simulating the year of 2008. Average prior variances for X_{CO2} and X_{CH4} after multiplied the factor were $(7.7 \text{ ppm})^2$ and $(0.087 \text{ ppm})^2$, respectively. The ground surface albedo was assumed to be represented by several grid values and to vary linearly from one grid value to the next. Using this processing sequence, it was possible to retrieve the X_{CO2} and X_{CH4} for any spectrum structure of the ground surface albedo in a flexible manner. The a priori and variance of the ground surface albedo were set to 0.2 and $(1.0)^2$, respectively, with a width of 25 cm⁻¹ to the adjacent grid. The a priori aerosol optical thickness was calculated by the Spectral Radiation-Transport Model for Aerosol Species (SPRINTARS; Takemura et al. 2000) and its variance was set to $(1.0)^2$. The relative radiometric calibration adjustment factor indicates the uncertainty in the prelaunch radiometric calibration and the degradation of the instrument after launch, and its a priori and a priori variance were set to 1.0 and $(0.01)^2$.

3. Results

The TANSO-FTS SWIR spectrum data for April 20–28, 2009, were selected for retrieval. During this period, GOSAT observed the entire globe three times in one of its nominal five-points observation mode operations; each five observation scenes of TANSO-FTS are arranged orthogonally to the GOSAT orbital path. Although there were approximately 87000 TANSO-FTS SWIR measurement scenes during this period, only about 1300 of these met the selection criteria described in Section 2.2, and were passed to the retrieval process. Over the ocean, GOSAT did not operate in sun-glint observation mode, which targets glint points along its orbit, and therefore no measurement scenes were available because of the low reflectivity of the ocean surface.

Figure 1 shows the global distribution of retrieved X_{CO2} and X_{CH4}. The retrieved scenes were primarily located in sub-tropical regions, because of the cloud-free condition imposed in selecting data. Figure 2 shows the latitudinal distributions of the zonal average of retrieved X_{CO2} and X_{CH4} along with the corresponding average values from NIES TM. The hemispheric gradients of X_{CO2} and X_{CH4} were consistent with the current state of knowledge on the subject (Schneising et al. 2008, 2009, and references therein), but the derived
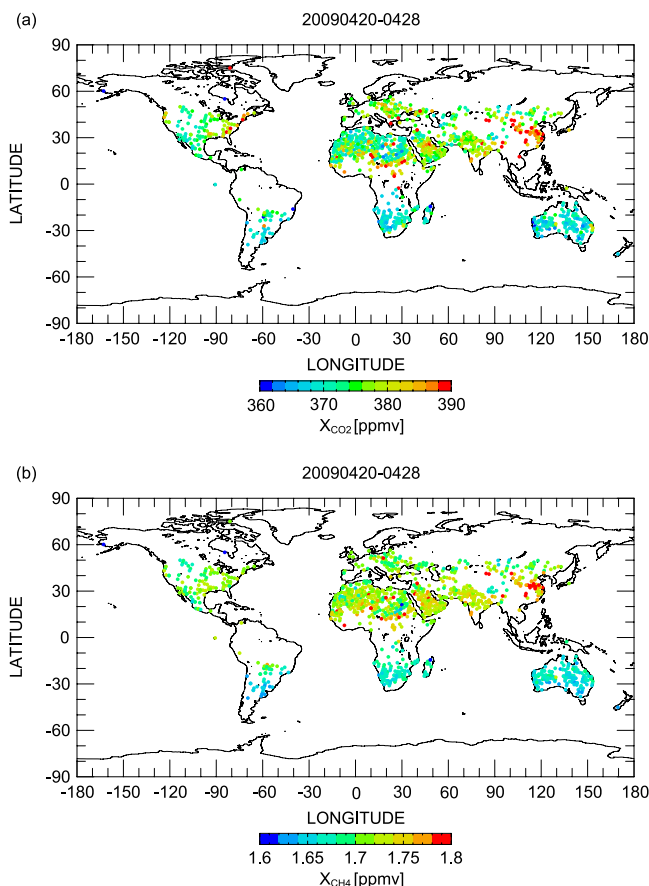
Fig. 1. Preliminary results of global distribution of (a) X_{CO2} and (b) X_{CH4} for April 20–28, 2009 retrieved from GOSAT TANSO-FTS SWIR spectra with SNR greater than 100 and for cloud-free scenes over land.

Fig. 2. Latitudinal distributions of zonal mean of (a) X_{CO2} and (b) X_{CH4} for April 20–28, 2009. Black crosses and vertical bars indicate the latitudinal average and standard deviation of the retrieved column-averaged dry air mole fractions with 15° latitudinal bands. Three crosses without a vertical bar have no statistical meaning because only one scene was retrieved at those latitudinal ranges. Gray squares indicate the corresponding a priori latitudinal average of column-averaged dry air mole fractions by NIES TM.

X_{CO2} and X_{CH4} values were generally lower than those predicted by NIES TM. This could be attributed to the uncertainty in the uncalibrated radiometric and geometric data. Intensive error analyses will be presented after confirming the calibration accuracy.

The seasonal variation of X_{CO2} is controlled mainly by photosynthesis in the terrestrial ecosystem, and this explains the larger X_{CO2} values in the northern hemisphere in late April (Schneising et al. 2008, and references therein). The retrieval results showed the average X_{CO2} in the northern hemisphere was about 10 ppm higher than that of the southern hemisphere, while the hemispheric gradient value simulated by NIES TM was 4 ppm. Unlike X_{CO2}, X_{CH4} showed larger values in the northern hemisphere than in the southern hemisphere throughout the whole year, due to the large natural and anthropogenic sources of CH_4 in the northern hemisphere (Schneising et al. 2009, and references therein). The retrieved results show that X_{CH4} in the northern hemisphere was about 0.05 ppm higher than that of the southern hemisphere. This agrees closely with the north-south difference based on the NIES TM calculation. The retrieved X_{CH4} was on average approximately 0.1 ppm lower than the NIES TM calculation.

High concentrations were observed for both X_{CO2} and X_{CH4} over continental China and Central Africa, possibly due to the presence of atmospheric dust. Asian dust (yellow sand) over continental China and dust or smoke-like phenomena in the some locations in Africa were
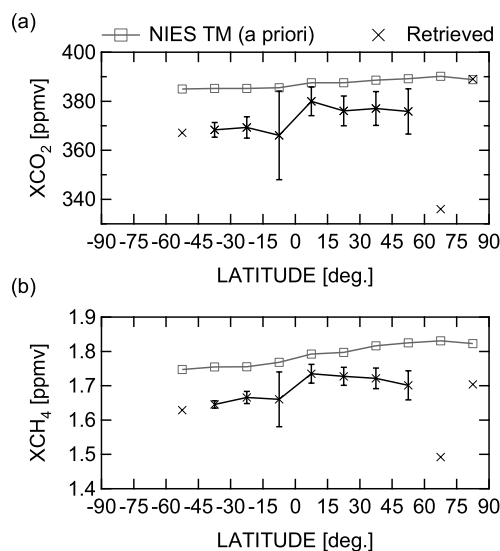
evident in TANSO-CAI images. The aerosol optical properties of TANSO-CAI, which are largely affected by the radiometric calibration accuracy of the instrument and not used in this study, will help distinguish the artificial bias due to aerosol from the actual variation of those gases.

4. Concluding remarks

This paper presents a first attempt at X_{CO2} and X_{CH4} retrieval from TANSO-FTS SWIR spectrum data under cloud-free conditions. Both X_{CO2} and X_{CH4} show a hemispheric gradient, with the largest values in the northern hemisphere, in general agreement with the current state of knowledge, despite uncalibrated spectrum data being used in the retrieval analyses. Validation and error analysis should be taken into account to improve the retrieval results, based on the results of radiometric and geometric calibration. After confirming the accuracy of calibration and the validation activities, we plan to release the calibrated measurement spectrum data (TANSO-FTS data) and the imager data (TANSO-CAI data) to the public nine months after the satellite launch (i.e., by late October 2009). We also plan to release the validated X_{CO2}, X_{CH4} and cloud coverage flag data three months later (i.e., by late January 2010).

Acknowledgments

Miyasaka of Fujitsu FIP Corporation. The transport model setup was prepared by Dmitry Belikov and Tazu Saeki at NIES and the a priori covariance matrix was prepared by Ryu Saito at NIES. The extended GPV dataset was provided to the GOSAT project by JMA. We dedicate this paper to the memory of our colleague, Tadao Aoki who initiated GOSAT SWIR retrieval algorithm development.

References

Eguchi, N., R. Saito, T. Saeki, Y. Nakatsuka, D. Belikov, and S. Maksyutov, 2009: A priori covariance estimation for CO_2 and CH_4 retrievals, *J. Geophys. Res. Atm.*, (submitted).

GLOVALVIEW-CH4, 2008: Cooperative Atmospheric Data Integration Project – Methane. CD-ROM, NOAA ESRL, Boulder, Colorado (Also available on Internet via anonymous FTP to ftp.cmdl.noaa.gov, Path: ccg/ch4/ GLOBALVIEW).

GLOVALVIEW-CO2, 2008: Cooperative Atmospheric Data Integration Project - Carbon Dioxide. CD-ROM, NOAA ESRL, Boulder, Colorado (Also available on Internet via anonymous FTP to ftp.cmdl.noaa.gov, Path: ccg/ co2/GLOBALVIEW).

IPCC, 2007: *Climate change 2007: The physical Science Basis. Contribution of Working Group I to the Fourth Assessment Report of the Intergovernmental Panel on Climate Change*, S. Solomon, D. Qin, M. Manning, Z. Chen, M. Marquis, K. B. Avervt, M. Tignor, and H. L. Miller, Eds., Cambridge University Press, Cambridge, United Kingdom and New York, NY, USA, 996 pp.

Kuze, A., K. Kondo, T. Hamazaki, and T. Urabe, 2006: The instrumentation and the BBM test results of thermal and near-infrared sensor for carbon observation (TANSO) on GOSAT, *Proc. SPIE, 6297, Infrared Spaceborne Remote Sensing XIV*.

Law, R. M., W. Peters, C. Rödenbeck, C. Aulagnier, I. Baker, D. J. Bergmann, P. Bousquet, J. Brandt, L. Bruhwiler, P. J. Cameron-Smith, J. H. Christensen, F. Delage, A. S. Denning, S. Fan, C. Geels, S. Houweling, R. Imasu, U. Karstens, S. R. Kawa, J. Kleist, M. C. Krol, S.-J. Lin, R. Lokupitiya, T. Maki, S. Maksyutov, Y. Niwa, R. Onishi, N. Parazoo, P. K. Patra, G. Pieterse, L. Rivier, M. Satoh, S. Serrar, S. Taguchi, M. Takigawa, R. Vautard, A. T. Vermeulen, and Z. Zhu, 2008: TransCom model simulations of hourly atmospheric CO_2: Experimental overview and diurnal cycle results for 2002, *Global Biogeochem. Cycles*, **22**, GB3009, doi:10.1029/2007GB 003050.

Maksyutov, S., P. K. Patra, R. Onishi, T. Saeki, and T. Nakazawa, 2008: NIES/FRCGC global atmospheric tracer transport model: Description, validation, and surface sources and sinks inversion, *J. Earth Simulator*, **9**, 3–18.

Nakajima, T., T. Y. Nakajima, A. Higurashi, I. Sano, T. Takamura, H. Ishida, and N. Schutgens, 2008: A study of aerosol and cloud information retrievals from CAI imager on board GOSAT satellite, *J. Remote Sens. Soc. Japan*, **28**, 178–189, (in Japanese with English abstract and figure captions).

Rodgers, C. D., 2000: *Inverse Methods for Atmospheric Sounding: Theory and Practice*, World Sci., Singapore.

Rodgers, C. D., and B. J. Connor, 2003: Intercomparison of remote sounding instruments, *J. Geophys. Res.*, **108** (D3), 4116, doi:10.1029/2002JD002299.

Rothman, L. S., I. E. Gordon, A. Barbe, D. C. Benner, P. F. Bernath, M. Birk, V. Boudon, L. R. Brown, A. Campargue, J.-P. Champion, K. Chance, L. H. Coudert, V. Dana, V. M. Devi, S. Fally, J.-M. Flaud, R. R. Gamache, A. Goldman, D. Jacquemart, I. Kleiner, N. Lacome, W. J. Lafferty, J.-Y. Mandin, S. T. Massie, S. N. Mikhailenko, C. E. Miller, N. Moazzen-Ahmadi, O. V. Naumenko, A. V. Nikitin, J. Orphal, V. I. Perevalov, A. Perrin, A. Predoi-Cross, C. P. Rinsland, M. Rotger, M. Šimečková, M. A. H. Smith, K. Sung, S. A. Tashkun, J. Tennyson, R. A. Toth, A. C. Vandaele, and J. V. Auwera, 2009: The HITRAN 2008 molecular spectroscopic database, *J. Quant. Spectrosc. Radiat. Transfer*, **110**, 533–572.

Patra, P. K., R. M. Law, W. Peters, C. Rödenbeck, M. Takigawa, C. Aulagnier, I. Baker, D. J. Bergmann, P. Bousquet, J. Brandt, L. Bruhwiler, P. J. Cameron-Smith, J. H. Christensen, F. Delage, A. S. Denning, S. Fan, C. Geels, S. Houweling, R. Imasu, U. Karstens, S. R. Kawa, J. Kleist, M. C. Krol, S.-J. Lin, R. Lokupitiya, T. Maki, S. Maksyutov, Y. Niwa, R. Onishi, N. Parazoo, G. Pieterse, L. Rivier, M. Satoh, S. Serrar, S. Taguchi, R. Vautard, A. T. Vermeulen, and Z. Zhu, 2008: TransCom model simulations of hourly atmospheric CO_2: Analysis of synoptic-scale variations for the period 2002–2003, *Global Biogeochem. Cycles*, **22**, GB4013, doi:10.1029/ 2007GB003081.

Patra, P. K., M. Takigawa, K. Ishijima, B.-C. Choi, D. Cunnold, E. J. Dlugokencky, P. Fraser, A. J. Gomez-Pelaez, T.-Y. Goo, J.-S. Kim, P. Krummel, R. Langenfelds, F. Meinhardt, H. Mukai, S. O'Doherty, R. G. Prinn, P. Simmonds, P. Steele, Y. Tohjima, K. Tsuboi, K. Uhse, R. Weiss, D. Worthy, and T. Nakazawa, 2009: Growth rate, seasonal, synoptic, diurnal variations and budget of methane in lower atmosphere, *J. Meteor. Soc. Japan*, **87**, 635–663.

Schneising, O., M. Buchwitz, J. P. Burrows, H. Bovensmann, M. Reuter, J. Notholt, R. Macatangay, and T. Warneke, 2008: Three years of greenhouse gas column-averaged dry air mole fractions retrieved from satellite – Part 1: Carbon dioxide, *Atmos. Chem. Phys.*, **8**, 3827–3853.

Schneising, O., M. Buchwitz, J. P. Burrows, H. Bovensmann, P. Bergamaschi, and W. Peters, 2009: Three years of greenhouse gas column-averaged dry air mole fractions retrieved from satellite – Part 2: Methane, *Atmos. Chem. Phys.*, **9**, 443–465.

Takemura, T., H. Okamoto, Y. Maruyama, A. Numaguti, A. Higurashi, and T. Nakajima, 2000: Global three-dimensional simulation of aerosol optical thickness distribution of various origins, *J. Geophys. Res.*, **105**, 17853–17873.

Yokota, T., H. Oguma, I. Morino, and G. Inoue, 2004: A nadir looking SWIR FTS to monitor CO_2 column density for Japanese GOSAT project, *Proc. Twenty-fourth Int. Sympo. on Space Technol. and Sci (Selected Papers), JSASS and Organizing Comm. of the 24th ISTS*, 887–889.